

Deterministic two-photon C-Z gate with the two-photon quantum Rabi model

Jia-Cheng Tang,¹ Jin Zhao,^{2,*} Haitao Yang,³ Junlong Tian,⁴ Pinghua Tang,¹ Shuai-Peng Wang,^{5,†} Lucas Lamata,^{6,‡} and Jie Peng^{1,§}

¹*Hunan Key Laboratory for Micro-Nano Energy Materials and Devices and School of Physics and Optoelectronics, Xiangtan University, Hunan 411105, China*

²*Hangzhou Institute for Advanced Study, UCAS, Hangzhou 310024, China*

³*School of physics and electronic information engineering, Zhaotong University, Zhaotong 657000, People's Republic of China*

⁴*Department of Electronic Science, College of Big Data and Information Engineering, Guizhou University, Guiyang 550025, China*

⁵*Beijing Academy of Quantum Information Sciences, Beijing 100193, China*

⁶*Departamento de Física Atómica, Molecular y Nuclear, Universidad de Sevilla, 41080 Sevilla, Spain*

We propose a scheme for realizing a deterministic two-photon C-Z gate based on variants of the two-photon quantum Rabi model (QRM), which is feasible within the framework of circuit QED. We begin by utilizing the two-photon interaction to implement the nonlinear sign (NS) gate, and subsequently, we construct the C-Z gate following the KLM scheme. We consider three different regimes: the strong coupling regime, the perturbative ultrastrong coupling regime, and the large detuning regime. Our results indicate that the C-Z gate operates fast with high fidelity, and is robust against decoherence. We also show the photonic state in the waveguide can be input into the circuit QED system through a variable coupler, and released after interaction with almost the same waveform except for a π -phase shift. Our scheme offers a suitable approach for achieving fast and deterministic two-photon quantum gates via light-matter interactions.

I. INTRODUCTION

Quantum computing offers advantages in certain fields due to its unique computational methods [1]. The power of quantum computing grows exponentially with the number of qubits involved in the computation, a feature that stems from the quantum properties of superposition and entanglement [2, 3]. A variety of physical systems have been explored for implementing quantum computing, including photons [4–7], trapped ions [8], nuclear magnetic resonance [9], quantum dots [10], cavity QED [11], and circuit QED [12, 13]. Among these, superconducting circuit QED systems [14, 15] and photonic quantum computation [16] have garnered significant attention due to substantial experimental and theoretical progress over the past two decades [17–19].

Universal quantum gates, which are essential components of a universal quantum computer, can be constructed using C-Z gates (or C-phase gates) in conjunction with a series of single-qubit rotations [1]. Compared to circuit QED systems, implementing a C-Z gate in a photonic system is more challenging due to the scarcity of nonlinearity. In 2001, Knill, Laflamme, and Milburn (KLM) proposed a complete linear optics quantum computing scheme [4]. They demonstrated that linear optics elements could be used to implement a nonlinear sign gate (NS gate), and a C-Z gate could be constructed using two NS gates. However, the NS gate and C-Z gate

in their scheme are nondeterministic, with success probabilities of $1/4$ and $1/16$, respectively, and they require extensive optical resources for scalability [6]. A significant challenge in constructing two-qubit logical gates in optical quantum computing is the introduction of optical nonlinearity. In the KLM scheme, the necessary nonlinearity is achieved through single-photon detection and postselection. Alternative methods for implementing NS gates and, consequently, C-Z gates have been proposed. An early approach involved Kerr-nonlinear photonic crystals [20]. In 2017, Costanzo et al. emulated the effect of strong Kerr nonlinearity on the quantum state of light using sequences and superpositions of single-photon additions and subtractions [21]. Others have introduced nonlinearity through photon-atom interactions [22–24]. In 2013, Adhikari et al. achieved a deterministic two-photon nonlinear phase shift in the microwave domain using a nonlinearly-coupled system between an LC resonator and a transmon qubit via an adiabatic scheme [25]. Another deterministic C-Z gate scheme, which exploited a nonlinear π -phase shift of two-photon molecule generations in chiral waveguide QED systems, was proposed in 2019 [26]. Additionally, several photonic quantum gates have been proposed in recent years [27–29].

In this article, we propose a scheme to realize a deterministic two-photon C-Z gate based on the two-photon quantum Rabi model (QRM). The QRM is extensively studied recently [30–37]. The two-photon QRM can be directly implemented in a circuit QED system with a sophisticated design by Felicetti et al. in 2018 [38, 39], where a flux qubit is inductively coupled to a SQUID. An effective two-photon QRM with arbitrary coupling strength can also be realized in circuit QED by adding a two-tone drive [40]. This two-photon interaction reveals

* zhaojin24@mailsucas.ac.cn

† wangsp@baqis.ac.cn

‡ llamata@us.es

§ jpeng@xtu.edu.cn

novel physical phenomena [41–44] and can be directly applied to introduce a two-photon nonlinear phase shift, thereby enabling the implementation of the NS gate. We consider three scenarios: first, the system is described by the two-photon Jaynes-Cummings (JC) model in the strong coupling (SC) regime; second, a Bloch-Siegert Hamiltonian is applied in the perturbative ultrastrong coupling (p-USC) regime; and third, a dispersive Hamiltonian is used to describe the system in the large detuning regime. We calculate the dynamics and find that a π -phase can be accumulated for the two-photon state, allowing for the realization of a two-photon NS gate in 1.4, 0.8, and 15 ns with high fidelity, respectively. Considering the full experimental process, we show the photonic states in the waveguide can be input into the cavity through a variable coupler, and released after interaction with the flux qubit. The waveform is almost kept the same, but a π -phase shift is added. We then use this to construct the two-photon C-Z gate according to the KLM scheme [4]. Furthermore, we demonstrate that our scheme is not only fast but also robust against decoherence [45].

II. TWO-PHOTON C-Z GATE IN THE STRONG COUPLING REGIME

The NS gate is a critical component of the C-Z gate within the KLM scheme [4]. It introduces a nonlinear π -phase shift specific to the two-photon component, which can be represented as the transformation $\alpha_0|0\rangle + \alpha_1|1\rangle + \alpha_2|2\rangle \rightarrow \alpha_0|0\rangle + \alpha_1|1\rangle - \alpha_2|2\rangle$. This effect is achieved through a nonlinear interaction between a qubit and a photonic mode. Typically, linear coupling prevails, but a two-photon quantum Rabi model can be implemented in circuit QED with a sophisticated design by Felicetti et al. [38]. This design involves a superconducting quantum interference device (SQUID) inductively coupled to a three-junction flux qubit. By connecting it to an input/output transmission line (TL) via a variable coupler, the realization of a two-photon NS gate becomes feasible, as depicted in Fig. 1.

The dynamics of the two-photon quantum Rabi model (QRM) encompass infinite-photon subspaces, complicating the direct realization of a two-photon gate. However, we can address this challenge within three specific regimes: the strong coupling (SC) regime, the perturbative ultrastrong coupling (p-USC) regime, and the large detuning regime. Here we focus on the first case, where the Hamiltonian can be effectively approximated by the two-photon Jaynes-Cummings (JC) Hamiltonian under the rotating-wave approximation ($\hbar = 1$)

$$H_{2JC} = \omega_r a^\dagger a + \frac{\omega_q}{2} \sigma_z + g(\sigma_+ a^2 + \sigma_- a^{\dagger 2}), \quad (1)$$

where $\omega_r = \sqrt{(C_{SQ}\Phi_0)/(4\pi I_c \cos(\pi\Phi_{\text{ext}}/\Phi_0))}$. C_{SQ} is the total capacitance of the SQUID and I_c is the critical current of the single Josephson junction. $\Phi_0 = h/(2e)$ is

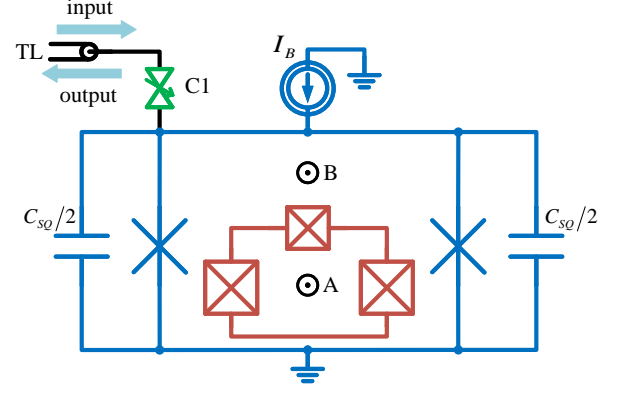


FIG. 1. Schematic diagram of the circuit QED setup to implement a NS gate. A three-junction flux qubit (red) is inductively coupled to a SQUID resonator (blue), which is biased by an external direct current I_B [38]. The SQUID is connected to an input/output transmission line (TL) via a variable coupler (green), enabling catching and releasing of photons with a controllable photon dissipation rate κ_c [46]. An external flux Φ_A threads the flux qubit in region A, and the larger loop of the SQUID outside region A is threaded by a flux Φ_B . Thus, the net external flux through the SQUID is $\Phi_{\text{ext}} = \Phi_B + \Phi_A$.

magnetic flux quantum. Φ_{ext} is the total magnetic flux threading the SQUID loop. $a^\dagger(a)$ is the photonic creation (annihilation) operator. ω_q is the transition energy of two lowest persistent-current states of the flux qubit which has been biased at the degeneracy point $\Phi_A = \Phi_0/2$ [47]. $\sigma_z = |e\rangle\langle e| - |g\rangle\langle g|$, with $|e\rangle$ and $|g\rangle$ denoting the left-circulating and right-circulating persistent-current states, respectively. $\sigma_+ = |e\rangle\langle g|$ and $\sigma_- = |g\rangle\langle e|$ are the raising and lowering operation of the flux qubit respectively. The coupling strength between the SQUID and the flux qubit $g = -(\pi/4)\tan(\pi\Phi_{\text{ext}}/\Phi_0)(MI_p/\Phi_0)\omega_r$, where I_p is the persisting current of the flux qubit and M is the coefficient of mutual inductance between two loops.

In the two-photon JC model, it is easy to find a symmetry operator $C_{2JC} = a^\dagger a + 2\sigma_+ \sigma_-$ commuting with H_{2JC} . The symmetry leads to exact solutions in subspaces spanned over the basis $\{|0, g\rangle\}, \{|1, g\rangle\}, \{|2, g\rangle, |0, e\rangle\} \dots \{|n, g\rangle, |n-2, e\rangle\}$. Transformed to the interaction picture with respect to $H_0 = \omega_r a^\dagger a + \omega_q/2 \sigma_z$, the Hamiltonian of the two-photon JC model reads

$$H_{2JC}^{\text{int}} = g(\sigma_+ a^2 e^{i\delta t} + \sigma_- a^{\dagger 2} e^{-i\delta t}). \quad (2)$$

Here, $\delta = \omega_q - 2\omega_r$ is the detuning between the qubit and two photons. We consider the resonant case and set $\omega_q = 2\omega_r$ accordingly. Suppose the input microwave photon state from the TL is an arbitrary superposition state $\alpha_0|0\rangle + \alpha_1|1\rangle + \alpha_2|2\rangle$ and the flux qubit has been cooled down to the ground state. First, we turn on the

variable coupler C to input the initial state

$$|\psi_0\rangle = (\alpha_0|0\rangle + \alpha_1|1\rangle + \alpha_2|2\rangle) \otimes |g\rangle. \quad (3)$$

The eigenstates $|0, g\rangle$ and $|1, g\rangle$, belonging to the zero-excitation and one-excitation subspaces respectively, are time-invariant. But in the two-excitation subspace $\{|2, g\rangle, |0, e\rangle\}$, the system will evolve in the form of Rabi oscillation, as shown in Fig. 2(a). By solving the Schrödinger equation, we obtain

$$|\psi(t)\rangle = \alpha_0|0, g\rangle + \alpha_1|1, g\rangle + \alpha_2(\cos(\sqrt{2}gt)|2, g\rangle - i\sin(\sqrt{2}gt)|0, e\rangle). \quad (4)$$

After resonant interaction with an operation time of $t = \pi/(\sqrt{2}g)$, the system will evolve into

$$\psi_{\text{ideal}} = |\psi(\frac{\pi}{\sqrt{2}g})\rangle = \alpha_0|0, g\rangle + \alpha_1|1, g\rangle - \alpha_2|2, g\rangle \quad (5)$$

Then we turn on C to release photons from the resonator into the TL as an output.

To evaluate the performance of the NS gate, we simulate the evolution of the system under environment dissipations with the Lindblad master equation [19]

$$\dot{\rho}(t) = -i[H_{2JC}^{int}, \rho] + \kappa D[a]\rho + \gamma D[\sigma_-]\rho + \frac{\gamma_\varphi}{2} D[\sigma_z]\rho, \quad (6)$$

where $D[L]\rho = (2L\rho L^\dagger - L^\dagger L\rho - \rho L^\dagger L)/2$ with $L = a, \sigma_-, \sigma_z$. κ is the dissipation rate of the SQUID resonator. γ is the energy relaxation rate of the qubit, and γ_φ is the dephasing rate of the qubit. The parameters are chosen as: $\omega_r/2\pi = \omega_q/4\pi = 5$ GHz, $g/2\pi = 0.25$ GHz, and $\kappa = \gamma = \gamma_\varphi = 0.05 \mu\text{s}^{-1}$ [19]. The simulation results in Fig. 2(b) shows that the fidelity of our NS gate $F = |\langle\psi_{\text{ideal}}|\rho(T)|\psi_{\text{ideal}}\rangle|$ is 99.95% within the operation time of $T = 2\pi/g \approx 1.4$ ns, which can be further reduced

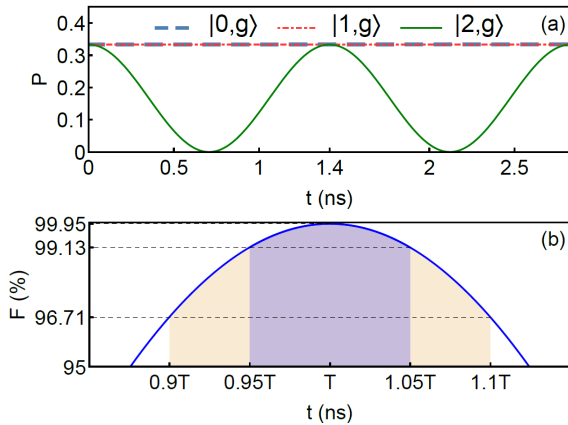


FIG. 2. (a) Time evolution governed by H_{2JC}^{int} with initial state $|\psi_0\rangle$ ($\alpha_0 = \alpha_1 = \alpha_2$ for simplicity). (b) Fidelity of the NS gate near the optimum time $T = 1.4$ ns. $\omega_r/2\pi = \omega_q/4\pi = 5$ GHz, $g/2\pi = 0.25$ GHz, and environment dissipations are $\kappa = \gamma = \gamma_\varphi = 0.05 \mu\text{s}^{-1}$.

to 0.7 ns at the SC limit ($g = 0.1\omega_r$). It is worth noting that the coherence time of flux qubit has reached 100 μs [12, 48], and the resonator lifetime has been extended to milliseconds [49]. We have also investigated the effect of deviations in the evolution time. Even with a $\pm 5\%$ deviation from the optimal point T , the fidelity remains above 99.13%, as depicted in Fig. 2(b). The influences of detuning and environment dissipations on fidelity are shown in Fig. 3. It can be seen that the fidelity is robust against these factors, although it is more sensitive to κ and γ_φ than to γ .

Next we construct the two-photon C-Z gate with the NS gate designed above, according to the KLM scheme [4] (Fig. 4). Quantum information is encoded on a two-rail photon qubit basis $\{|0\rangle_1|0\rangle_2, |0\rangle_1|1\rangle_2, |1\rangle_1|0\rangle_2, |1\rangle_1|1\rangle_2\}$. Since the total photon number is conserved, the involved photonic states include $\{|00\rangle, |01\rangle, |10\rangle, |02\rangle, |11\rangle, |20\rangle\}$. The beam-splitters (BS) used to separate and mix microwave light [52] can be described by an unitary matrix

$$U(\theta) = \begin{pmatrix} 1 & 0 & 0 & 0 & 0 & 0 \\ 0 & -\sin\theta & \cos\theta & 0 & 0 & 0 \\ 0 & \cos\theta & \sin\theta & 0 & 0 & 0 \\ 0 & 0 & 0 & \sin^2\theta & -\sqrt{2}\sin\theta\cos\theta & \cos^2\theta \\ 0 & 0 & 0 & -\sqrt{2}\sin\theta\cos\theta & \cos^2\theta - \sin^2\theta & -\sqrt{2}\sin\theta\cos\theta \\ 0 & 0 & 0 & \cos^2\theta & -\sqrt{2}\sin\theta\cos\theta & \sin^2\theta \end{pmatrix}. \quad (7)$$

The unitary transformation matrix of a 50/50 beam-splitter corresponds to $U(\pi/4)$. To implement a C-Z gate, we must add a minus sign on $|11\rangle$ while keep other logical basis unchanged. This can be done as follows. First, the 50/50 BS makes $|11\rangle \rightarrow (|02\rangle + |20\rangle)/\sqrt{2}$ because of

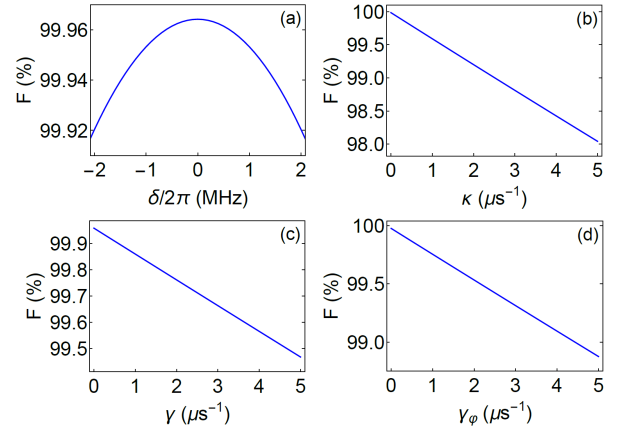


FIG. 3. The impact of detuning and environment dissipations on the fidelity F of the NS gate. (a) F as a function of the detuning δ between the photon and qubit frequencies, where $\kappa = \gamma = \gamma_\varphi = 0.05 \mu\text{s}^{-1}$. (b) F as a function of the resonator dissipation rate, where $\delta/2\pi = 1$ MHz, $\gamma = \gamma_\varphi = 0.05 \mu\text{s}^{-1}$. (c) F as a function of the energy relaxation rate γ of the qubit, where $\delta/2\pi = 1$ MHz, $\kappa = \gamma_\varphi = 0.05 \mu\text{s}^{-1}$. (d) F as a function of the dephasing rate of the qubit, where $\delta/2\pi = 1$ MHz, $\kappa = \gamma = 0.05 \mu\text{s}^{-1}$.

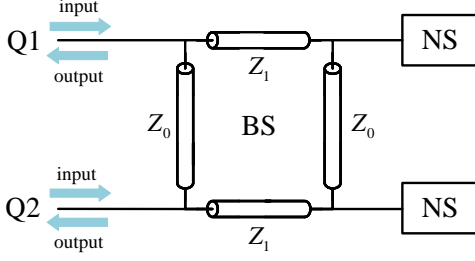


FIG. 4. Schematic diagram of two-photon C-Z gate. Four $\lambda/4$ sections of TL with impedance Z_0 and $Z_1 = Z_0/\sqrt{2}$ realize a 50:50 beam-splitter [50, 51]. Q1, Q2 act as both input and output ports of the C-Z gate. The NS gate is realized according to the design in Fig. 1

HOM interference [52]. Then, two NS gates are used to introduce a π -phase shift: $|02\rangle + |20\rangle \rightarrow -|02\rangle - |20\rangle$. The output photonic state goes through the same beam-splitter again and becomes $-|11\rangle$. Other logical basis $\{|00\rangle, |01\rangle, |10\rangle\}$ will not be changed by the NS gate [53]. Therefore, a C-Z gate is implemented.

Next we consider the effect of the environment including the resonator dissipation, qubit damping and dephasing, and the imperfection of the beam-splitter. We choose initial state $|\phi_0\rangle = (|00\rangle + |01\rangle + |10\rangle + |11\rangle)/2$, and define the fidelity of the C-Z gate as $F = |\langle\phi_{\text{ideal}}|\rho_{\text{out}}|\phi_{\text{ideal}}\rangle|$ with $|\phi_{\text{ideal}}\rangle = (|00\rangle + |01\rangle + |10\rangle - |11\rangle)/2$. According to the master equation (6), F reaches 99.89% when $\omega_r/2\pi = \omega_q/4\pi = 5$ GHz, $\kappa = \gamma = \gamma_\varphi = 0.05 \mu\text{s}^{-1}$, and $\theta = \pi/4 + 0.01$. We have also depicted the input and output state density matrices in Fig. 5, which show our scheme is efficient and robust against decoherence.

III. TWO-PHOTON C-Z GATE IN THE PERTURBATIVE ULTRAstrong COUPLING REGIME

In this section, we realize the two-photon C-Z gate in the perturbative ultrastrong coupling (p-USC) regime of the two-photon QRM, where $g(\bar{n} + 1) \ll \omega_q, \omega_q + 2\omega_r$. Here $\bar{n} \leq 2$ for arbitrary initial photonic state (3). In this regime, the two-photon QRM reduces to the two-photon Bloch-Siegert Hamiltonian [38]

$$H_{2BS} = H_{2JC} - \omega_{2BS} a^\dagger a + \left(\frac{\omega_{2BS}}{2} + \frac{\Omega_q}{2}\right) \sigma_z + \left(\frac{\omega_{2BS}}{2} + 2\Omega_q\right) \sigma_z (a^\dagger a + (a^\dagger a)^2), \quad (8)$$

where $\omega_{2BS} = 2g^2/(2\omega_r + \omega_q)$ and $\Omega_q = 2g^2/\omega_q$ are the two-photon Bloch-Siegert shifts [54, 55]. Choosing

$$H_0 = (\omega_r - \omega_{2BS}) a^\dagger a + \left(\frac{\omega_q}{2} + \frac{\omega_{2BS}}{2} + \frac{\Omega_q}{2}\right) \sigma_z, \quad (9)$$

we obtain

$$H_{2BS}^{\text{int}} = \left(\frac{\omega_{2BS}}{2} + 2\Omega_q\right) \sigma_z (a^\dagger a + (a^\dagger a)^2) + g(\sigma_+ a^2 e^{i(\omega_q - 2\omega_r + 3\omega_{2BS} + \Omega_q)t} + H.c.) \quad (10)$$

in the interaction picture. To make it time-independent, we choose $\omega_q - 2\omega_r + 3\omega_{2BS} + \Omega_q = 0$. So that

$$\frac{g}{\omega_r} = \frac{\sqrt{4r - r^3}}{2\sqrt{1 + 2r}}, \quad (11)$$

where $r = \omega_q/\omega_r$. Now the total excitation number operator $a^\dagger a + 2\sigma_+ \sigma_-$ is still conserved. For initial state (3), the involved Hilbert space consists of $\{|0, g\rangle, |1, g\rangle, |0, e\rangle, |2, g\rangle\}$, and H_{2BS}^{int} reads

$$\begin{pmatrix} 0 & 0 & 0 & 0 \\ 0 & B/3 & 0 & 0 \\ 0 & 0 & 0 & \sqrt{2}g \\ 0 & 0 & \sqrt{2}g & B \end{pmatrix}, \quad (12)$$

where $B = -6(\omega_{2BS}/2 + 2\Omega_q)$ is a function of r . By solving the Schrödinger equation analytically, we obtain

$$\begin{aligned} |\psi(t)\rangle &= \alpha_0 |0, g\rangle + \alpha_1 e^{-i\frac{B}{3}t} |1, g\rangle \\ &+ \alpha_2 e^{-i\frac{B}{2}t} \left[\frac{-i2\sqrt{2}g \sin(\frac{1}{2}\sqrt{B^2 + 8g^2}t)}{\sqrt{B^2 + 8g^2}} |0, e\rangle \right. \\ &\left. + \left(\cos(\frac{1}{2}\sqrt{B^2 + 8g^2}t) - \frac{iB \sin(\frac{1}{2}\sqrt{B^2 + 8g^2}t)}{\sqrt{B^2 + 8g^2}} \right) |2, g\rangle \right]. \end{aligned} \quad (13)$$

It can be seen that $|0, g\rangle$ is unchanged, and $|1, g\rangle$ will acquire a phase of $-Bt/3$. $|2, g\rangle$ will oscillate with $|0, e\rangle$ and acquire a phase of $-BT/2 + \pi$ after the population oscillation of a period $T = 2\pi/\sqrt{B^2 + 8g^2}$ in the two-dimensional subspace $\{|2, g\rangle, |0, e\rangle\}$ [See Fig. 6(a)]. Unlike the two-photon JC model, here the population can not be completely transferred. Supposing $t = kT$, the acquired phase for $|0, g\rangle$, $|1, g\rangle$ and $|2, g\rangle$ reads

$$\theta_0 = 0, \quad (14)$$

$$\theta_1 = -\frac{B}{3}kT, \quad (15)$$

$$\theta_2 = -\frac{B}{2}kT + k\pi, \quad (16)$$

respectively. To realize the NS gate, it is required that

$$\theta_1 - \theta_0 = 2n\pi, \quad (17)$$

$$\theta_2 - \theta_0 = (2m + 1)\pi, \quad (18)$$

where k, n and m are integers. The minimum $t = kT$ satisfying Eqs. (17) and (18) reads

$$kT = 6\pi/B, \quad k \text{ being even}, \quad (19)$$

$$kT = 12\pi/B, \quad k \text{ being odd}. \quad (20)$$

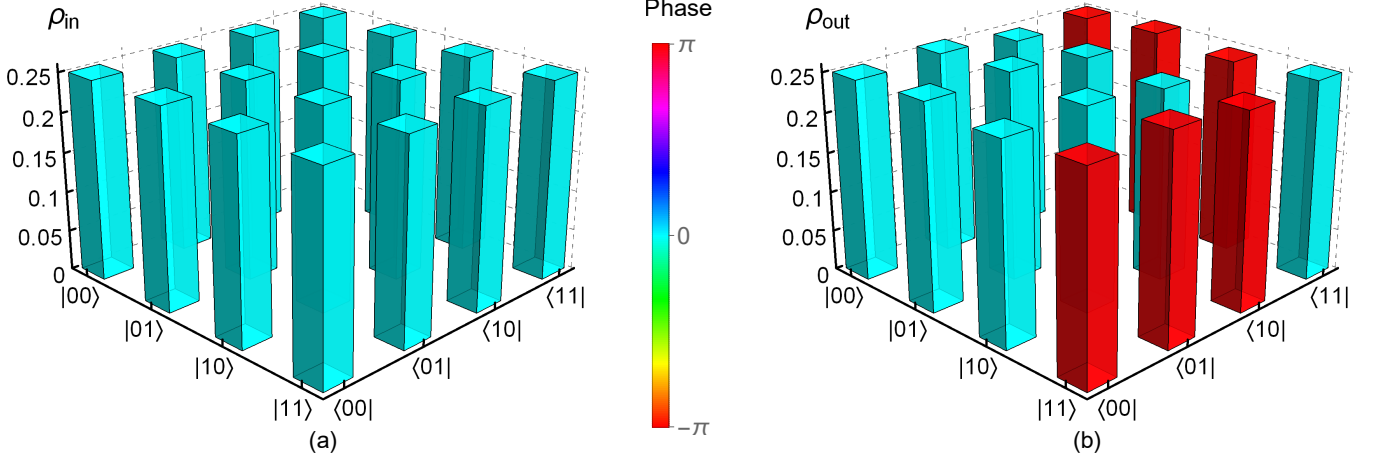


FIG. 5. (a) Density matrix ρ_{in} of input state $|\psi_{\text{in}}\rangle = |00\rangle + |01\rangle + |10\rangle + |11\rangle$. (b) Density matrix ρ_{out} . Here, we choose the environment parameters $\gamma = \kappa = \gamma_{\varphi} = 0.05 \mu\text{s}^{-1}$, and the beam-splitter parameter $\theta = \pi/4 + 0.01$.

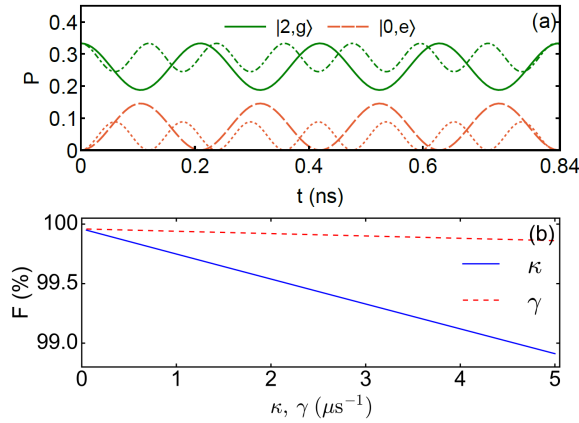


FIG. 6. (a) Dynamical evolution governed by H_{2BS}^{int} . $\omega_r/2\pi = 5\text{GHz}$, and $\kappa = \gamma = 0.05 \mu\text{s}^{-1}$. The solid and dashed oscillations correspond to the parameters $\omega_q/\omega_r = 1.87$ and $g/\omega_r = 0.223$ for $k = 4$, while the dot-dashed and dotted oscillations correspond to the parameters $\omega_q/\omega_r = 1.742$ and $g/\omega_r = 0.306$ for $k = 7$. A nonlinear π -phase shift is realized after 4 and 7 oscillations respectively. (b) Effects of the environment on the fidelity of the C-Z gate with the parameters of $k = 4$.

Since T and B are both functions of r , Eqs. (19) and (20) can be combined as

$$\frac{k}{3 + (-1)^{k+1}} = \frac{(1 + 2r)}{2(2 - r)(8 + 5r)} \times \sqrt{\frac{(2 - r)(1152 - r(-880 + r(230 + 209r)))}{(1 + 2r)^2}}. \quad (21)$$

Since $r = \omega_q/\omega_r > 0$, $k = 4, 6, 7, 8, 9, \dots$ to satisfy Eq. (21). Once k is fixed, we can obtain ω_q/ω_r , g/ω_r and gate time t in unit of ω_r^{-1} , as shown in Tab. 1. We plot the population of $|2, g\rangle$ and $|0, e\rangle$ for $k = 4$ and 7 in

Fig. 6(a). Once the NS gate is realized, the C-Z gate can be constructed with the same way as in the last section.

Finally, we study the dissipative dynamics in p-USC regime with dressed-state master equation [56, 57]

$$\dot{\rho}(t) = -i[H_{2BS}^{\text{int}}, \rho(t)] + \sum_{j,k>j} (\Gamma_{\kappa}^{jk} + \Gamma_{\gamma}^{jk})(D(|j\rangle\langle k|)\rho(t)), \quad (22)$$

where $D(L)\rho = (2L\rho L^{\dagger} - L^{\dagger}L\rho - \rho L^{\dagger}L)/2$, and $\{|j\rangle\}_{j=0,1,2,\dots}$ are eigenstates of the Hamiltonian H_{2BS} with eigenenergy ϵ_j . The decay rates read

$$\Gamma_{\kappa}^{jk} = \kappa \frac{\Delta_{kj}}{\omega_r} |\langle k|(a + a^{\dagger})|j\rangle|^2, \quad (23)$$

$$\Gamma_{\gamma}^{jk} = \gamma \frac{\Delta_{kj}}{\omega_q} |\langle k|\sigma_x|j\rangle|^2, \quad (24)$$

where $\Delta_{kj} = \epsilon_k - \epsilon_j$. The numerical results show the C-Z gate fidelity is robust against decoherence, as depicted in Fig. 6(b).

Here H_0 (9) is used in our interaction picture. If we replace it with a commonly used $H_0 = \omega_r a^{\dagger}a + \omega_q/2 \sigma_z$, we can also construct the NS gate with the same steps. In this way, the resonance condition is fixed at $\omega_q = 2\omega_r$, and the relationship between g and gate time t can also be obtained by repeating the above derivation,

$$\frac{k}{3 + (-1)^{k+1}} = \frac{\sqrt{2}\omega_r}{g} \sqrt{1 + 32\left(\frac{g}{\omega_r}\right)^2}, \quad (25)$$

$$t = \frac{k\pi}{\sqrt{2}g\sqrt{1 + 32(g/\omega_r)^2}}. \quad (g(\bar{n} + 1) \ll \omega_q) \quad (26)$$

However, the fastest gate time is about 3.6 ns with $g = 0.236\omega_r$ and $k = 20$, which is longer than that in the previous result.

k	r	$\omega_q/(2\pi)$ (GHz)	$g/(2\pi)$ (GHz)	t (ns)	F (%)
4	1.870	9.35	1.115	0.84	99.95
6	1.964	9.82	0.595	3.1	99.90
7	1.742	8.71	1.53	0.83	99.95
8	1.982	9.91	0.42	6.2	99.83
9	1.916	9.58	0.9	2.6	99.92

TAB. 1. Parameters correspond to different solutions k and r . For each set of parameters, the fidelity and gate time of the C-Z gate are also provided. $\omega_r/2\pi=5$ GHz, $\kappa=\gamma=\gamma_\varphi=0.05\ \mu\text{s}^{-1}$ and the beam-splitter $\theta=\pi/4+0.01$.

IV. TWO-PHOTON C-Z GATE IN THE DISPERSIVE REGIME

Finally, we propose a scheme to realize the C-Z gate with the two-photon QRM in the dispersive regime. When the frequencies of the resonator mode and the qubit are far detuned, the system can be described by a dispersive Hamiltonian, which is widely used for qubit readout in circuit QED [58, 59]. The two-photon QRM in the dispersive regime, i.e., $|\delta|=|\omega_q-2\omega_r|\gg g(\bar{n}+1)$, is given by [38]

$$H_{2JC}^{dis}=(\omega_r+\chi)a^\dagger a+(\omega_q+\chi)\frac{\sigma_z}{2}+\frac{\chi}{2}\sigma_z(a^\dagger a+(a^\dagger a)^2), \quad (27)$$

with $\chi=2g^2/|\delta|$. The last term in Eq. (27) consists of a nonlinear Kerr term that depends on the qubit state. Now the Hamiltonian is much simplified and one can easily obtain

$$\begin{aligned} |\psi(t)\rangle &= \alpha_0 e^{-iE_0 t}|0, g\rangle + \alpha_1 e^{-iE_1 t}|1, g\rangle + \alpha_2 e^{-iE_2 t}|2, g\rangle \\ &= \alpha_0 e^{i\frac{1}{2}(\omega_q+\chi)t}|0, g\rangle + \alpha_1 e^{i(\frac{1}{2}(\omega_q+\chi)-\omega_r)t}|1, g\rangle \\ &\quad + \alpha_2 e^{i(\frac{1}{2}(\omega_q+3\chi)-2\omega_r)t}|2, g\rangle, \end{aligned} \quad (28)$$

with initial state (3). To realize the nonlinear π -phase shift of the NS gate, the gate time t satisfies

$$\Delta E_{01}t=(E_1-E_0)t=\omega_r t=2n\pi, \quad (29)$$

$$\Delta E_{12}t=(E_2-E_1)t=(\omega_r-\chi)t=(2m-1)\pi, \quad (30)$$

$$\frac{\Delta E_{01}}{\Delta E_{12}}=\frac{\omega_r}{\omega_r-\chi}=\frac{2n}{2m-1}, \quad (31)$$

where n and m are integers. Since χ is normally smaller than ω_r in the dispersive regime, $2n>2m-1$. $\chi/\omega_r=(2n-2m+1)/2n$. To make parameters more practical in experiment, we chose $n=m$ to minimize $\chi/\omega_r=1/2n$ as plotted in Fig. 7(a). Considering $t=2n\pi/\omega_r$, we obtain

$$\frac{g}{\omega_r}=\frac{(\bar{n}+1)\pi}{2t\omega_r}\frac{|\delta|}{g(\bar{n}+1)}, \quad (32)$$

$$\frac{\omega_q}{\omega_r}=\frac{5(\bar{n}+1)^2\pi}{t\omega_r}\frac{|\delta|}{g(\bar{n}+1)}+2. \quad (33)$$

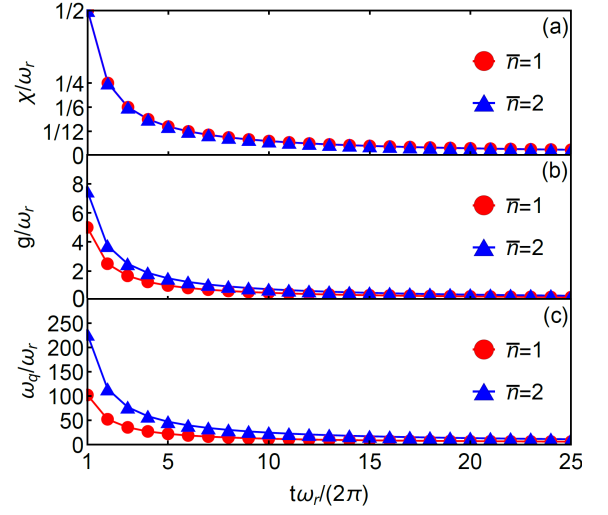


FIG. 7. (a)(b)(c) Relationship between C-Z gate time t and χ , g , and ω_q .

Since $|\delta|/(g(\bar{n}+1))\gg 1$, we chose it as 10 to depict the relationship between the gate time and g/ω_r for $\bar{n}=1$ and 2 in Fig. 7(b). It can be seen that the fastest time reaches $2\pi/\omega_r$. However, a large $g/\omega_r=5$ is required. The gate time reaches $20\pi/\omega_r$ when $g=0.5\omega_r$. Meanwhile, since $|\delta|/(g(\bar{n}+1))$ is chosen as 10, we obtain ω_q/ω_r , and depicted it in Fig. 7(c) for $\bar{n}=1$ and 2. One can choose suitable g , ω_r and ω_q in experiment to realize the C-Z gate with operation time shown in Fig. 7.

Considering realistic experimental conditions, we choose $\omega_r/2\pi=1$ GHz and $|\delta|=|\omega_q-2\omega_r|=10\omega_r$. Therefore, $g=\sqrt{|\delta|\omega_r/4n}$, taking into account that $\chi/\omega_r=1/2n$. The resonator dissipation rate and qubit damping rate are chosen as $\kappa=\gamma=0.01\ \mu\text{s}^{-1}$. We have also considered the imperfection of the beam-splitter by choosing the angle $\theta=\pi/4+0.01$. Then, we show the relationship between gate time t , fidelity F and χ/ω_r in Fig. 8(a), by using the dressed master equation (6). Finally, we choose one of the appropriate parameters in Fig. 8(a) ($\chi/\omega_r=1/36$, $|\delta|/\omega_r=10$, $g/\omega_r=0.395$), to consider the effect of the environment. Interestingly, the fidelity decreases with κ but will not change with γ , as depicted in Fig. 8(b). This is because the qubit is set to the ground state initially and there is not qubit transition terms in H_{2JC}^{dis} (27). Therefore it will always stay in the ground state, thus avoiding the effect of damping.

An advantage of dispersive coupling is that it can be used to implement the C-phase gate directly. It does not cause population oscillation, and add an arbitrary phase before $|2, g\rangle$. A C-phase gate can be realized if we replace $(2m-1)\pi$ with an arbitrary ϕ in Eq. (30).

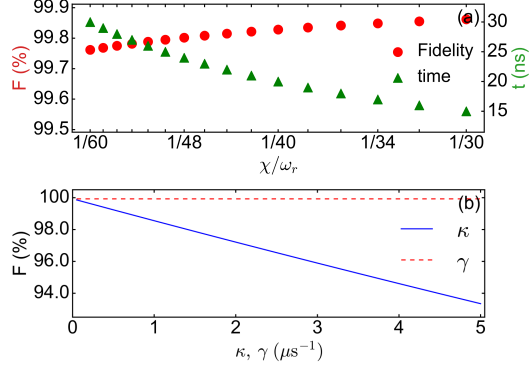


FIG. 8. (a) Fidelity and operation time of the C-Z gate. Simulation fidelity: red dots; gate time: green triangles. $\omega_r/2\pi = 1$ GHz, $\omega_q/2\pi = 12$ GHz. The environment dissipation parameters $\gamma = \kappa = 0.01 \mu\text{s}^{-1}$, and the beam-splitter $\theta = \pi/4 + 0.01$. (b) Environment effects on the fidelity of the C-Z gate. $\omega_r/2\pi = 1$ GHz, $\omega_q/2\pi = 12$ GHz, $g/2\pi = 0.395$ GHz.

V. INPUT AND OUTPUT OF THE PHOTONIC STATES

So far we only consider the interaction between the qubit and photon in the circuit QED system, however, the input and out put of the photonic states must be included in the whole experiment process. First, we must transfer the photonic state $|\phi\rangle$ like $\alpha_0|0\rangle_w + \alpha_1|1\rangle_w + \alpha_2|2\rangle_w$ in the waveguide to the circuit. Normally, $|\phi\rangle$ is not an ideal plane wave, but a Lorentz wave packet centered at ω_0 with finite bandwidth ϵ [60–62], therefore

$$|1\rangle_w = \int_0^\infty d\omega \mathcal{A} \frac{1}{\omega - \omega_0 - i\epsilon} b_\omega^\dagger |0\rangle, \quad (34)$$

$$|2\rangle_w = \int_0^\infty d\omega \int_0^\infty d\omega' \mathcal{B} \left(\frac{1}{\omega - \omega_0 + i\epsilon} \frac{1}{\omega' - \omega'_0 + i\epsilon} + \frac{1}{\omega' - \omega_0 + i\epsilon} \frac{1}{\omega - \omega'_0 + i\epsilon} \right) b_\omega^\dagger b_{\omega'}^\dagger |0\rangle, \quad (35)$$

where b_ω^\dagger and $b_{\omega'}^\dagger$ are creation operators of the waveguide mode with frequency ω and ω' respectively. \mathcal{A} and \mathcal{B} are normalizing constants. $|2\rangle_w$ takes this form to satisfy the permutation symmetry of the bosons. For simplicity, we consider two photons have the same center frequency resonant with the resonator $\omega_0 = \omega'_0 = \omega_r$.

The input and output process is as follows. First we turn off the resonator-qubit coupling to input $|\phi\rangle$ to the resonator, so that the Hamiltonian reads

$$H = \omega_r a^\dagger a + \int_0^\infty d\omega \omega b_\omega^\dagger b_\omega + g'_{wr} \int_0^\infty d\omega (a^\dagger b_\omega + b_\omega^\dagger a), \quad (36)$$

where g'_{wr} is the coupling between the waveguide and resonator. In the interaction picture with respect to $H_0 = \omega_r (a^\dagger a + \int_0^\infty d\omega b_\omega^\dagger b_\omega)$, the interaction Hamiltonian reads

$$H_I = \int_0^\infty d\omega \Delta_\omega b_\omega^\dagger b_\omega + g'_{wr} \int_0^\infty d\omega (a^\dagger b_\omega + b_\omega^\dagger a). \quad (37)$$

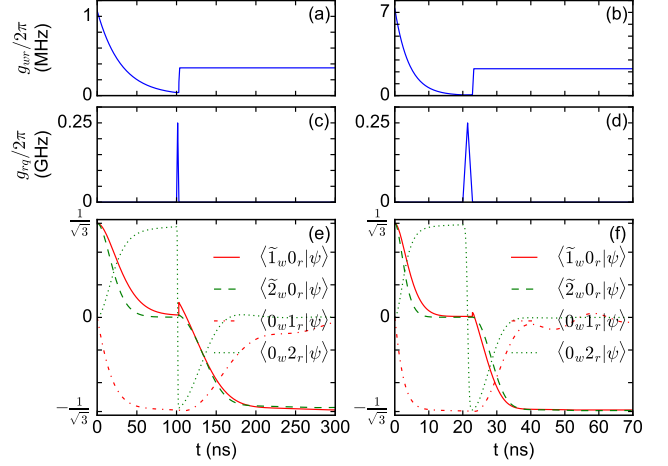


FIG. 9. Numerical simulation of the input and output process of $|\phi\rangle = \frac{1}{\sqrt{3}}(|0\rangle_w + |1\rangle_w + |2\rangle_w)$ as a Lorentz wavepacket with width 0.02 GHz (left panel) and 0.15 GHz (right panel). The parameters are optimized to ensure the success of this process, and shown in (a), (b), (c) and (d). We project instantaneous state $|\psi(t)\rangle$ into $|\tilde{1}\rangle_w|0\rangle_r$, $|\tilde{2}\rangle_w|0\rangle_r$, $|0\rangle_w|1\rangle_r$ and $|0\rangle_w|2\rangle_r$ to show the input and output process in (e) and (f). These projections are real because the imaginary parts are vanishing small.

where $\Delta_\omega = \omega - \omega_r$. The excitation number is conserved, so that

$$|\psi(t)\rangle = A(t)|2\rangle_r|0\rangle_w + \int_0^\infty d\omega B_\omega(t)|1\rangle_r|1_\omega\rangle + \int_0^\infty d\omega \int_0^\infty d\omega' C_{\omega,\omega'}(t)|0\rangle_r|1_\omega, 1_{\omega'}\rangle, \quad (38)$$

with $|\psi(0)\rangle = |0\rangle_r|\phi\rangle$, where $|i\rangle_r$ denotes i photons in the resonator. We aim to obtain $|\psi(t_{in})\rangle = |0\rangle_w(\alpha_0|0\rangle_r + \alpha_1|1\rangle_r + \alpha_2|2\rangle_r)$, however, it seems impossible to transfer all the population in a multimode state $|\phi\rangle$ into a single mode state with a constant coupling. Therefore, we introduce a variable coupler proposed by Yin et al. [46] which connects the waveguide and the resonator. Initially, their coupling g_{wr} is large, so that the population is quickly transferred from the waveguide to the resonator. Then we gradually decrease g_{wr} close to 0, to prevent the accumulated population in the resonator goes back to the waveguide. By optimizing g_{wr} , we can input the waveguide photonic state $|\phi\rangle$ to the resonator. Then we turn on the qubit-resonator coupling g_{rq} to add a π -phase shift to the two-photon part. Finally, we turn on g_{wr} again to output the photonic state to complete the NS gate. We need to optimize g_{wr} again to ensure the output photon waveform keeps the same as the input one, except for a π -phase shift.

Next we testify our proposal by numerical simulations. First we discrete the waveguide modes by introducing a finite but small frequency interval $\delta\omega = k\epsilon/N$ between two adjacent modes $|1_{\omega_m}\rangle_w$ and $|1_{\omega_{m+1}}\rangle_w$ [29], such that

the interaction Hamiltonian becomes

$$H_I = \sum_m \Delta_{\omega_m} b_{\omega_m}^\dagger b_{\omega_m} + g_{wr} \sum_m (a^\dagger b_{\omega_m} + b_{\omega_m}^\dagger a). \quad (39)$$

We chose $N = 100$, and the center frequency equalling ω_r . Then we solve the Schrödinger equation to obtain $|\psi\rangle$ and optimize g_{wr} accordingly. We consider two kinds of input Lorentz wavepackets with $\alpha_0 = \alpha_1 = \alpha_2 = 1/\sqrt{3}$: 1. $\epsilon = 0.02$ GHz, $k = 5$. 2. $\epsilon = 0.15$ GHz, $k = 4$. The numerical results are shown in the left and right panel of Fig. 9 respectively, where we define

$$|\tilde{i}\rangle_w = \begin{cases} \exp(-iH_{I0}t)|i\rangle_w & t < t_{in} + t_q, \\ \exp(-iH_{I0}(t - t_{in} - t_q))|i\rangle_w & t \geq t_{in} + t_q \end{cases} \quad (40)$$

for $i = 1, 2$ to include the free evolution of the photonic states in the waveguide with $H_{I0} = \sum_m \Delta_{\omega_m} b_{\omega_m}^\dagger b_{\omega_m}$. t_q is the qubit-resonator interaction time. The population of the waveguide modes almost vanishes at $t_{in} + t_q$, so that the accumulated dynamical phase is eliminated and $\exp(-iH_{I0}t)$ restart action when g_{wr} is turned on again at $t = t_{in} + t_q$. We project $|\psi\rangle$ into $|\tilde{1}\rangle_w|0\rangle_r$, $|\tilde{2}\rangle_w|0\rangle_r$, $|0\rangle_w|1\rangle_r$ and $|0\rangle_w|2\rangle_r$ to show the input and output process in Figs. 9 (e) and (f). The imaginary part is vanishing small, so that these projections are real.

When $\epsilon = 0.02$ GHz, $|\phi\rangle|0\rangle_r$ is transferred to $\frac{1}{\sqrt{3}}|0\rangle_w(|0\rangle_r - |1\rangle_r + |2\rangle_r)$ in $t_{in} = 100$ ns, as shown in Fig. 9 (e). The minus sign before $|0\rangle_w|1\rangle_r$ coincides with the single-photon resonant scattering result in waveguide QED [60–62], which can be eliminated by a linear phase shifter. Or else, one can interchange the definition of $|0\rangle$ and $|1\rangle$, then the C-Z gate can be realized subject to a trivial global phase π [27]. $g_{wr}/2\pi = 1.07 \exp(-0.0333t)$ MHz, as depicted in Fig. 9 (a). g_{rq} is then turned on as

$$g_{rq}(t) = \begin{cases} 2g_0(t - t_{in})/t_q & t_{in} < t < t_{in} + t_q/2, \\ -2g_0(t - t_{in} - t_q)/t_q & t_{in} + t_q/2 \leq t \leq t_{in} + t_q, \\ 0 & t < t_{in} \text{ \& } t > t_{in} + t_q, \end{cases} \quad (41)$$

where $g_0/2\pi = 0.25$ GHz, as depicted in Fig. 9 (c). We consider the strong qubit-resonator coupling regime, where the wavefunction of the circuit QED system reads

$$|\psi(t)\rangle = \cos\left(\sqrt{2} \int_0^t g_{rq}(t') dt'\right) |2, g\rangle - i \sin\left(\sqrt{2} \int_0^t g_{rq}(t') dt'\right) |0, e\rangle. \quad (42)$$

Since $g_{rq}(t)$ is linear, a π -phase is accumulated for the two-photon part in $t_q = \sqrt{2}\pi/g_0 = 2.8$ ns. When $t > t_{in} + t_q$, g_{rq} is turned off and $g_{wr}/2\pi$ is linearly increase to 0.35 MHz to release the $\alpha_0|0\rangle_r - \alpha_1|1\rangle_r - \alpha_2|2\rangle_r$ to the waveguide. Since we have optimized g_{wr} , the output photonic waveform is almost the same as the input

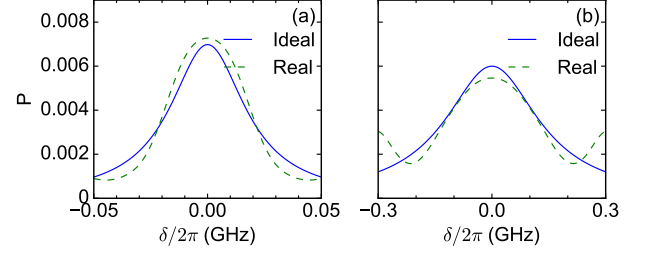


FIG. 10. Waveform of the input (ideal) and output (real) single-photon part of the photonic state in the waveguide. (a) $\epsilon = 0.02$ GHz. (b) $\epsilon = 0.15$ GHz.

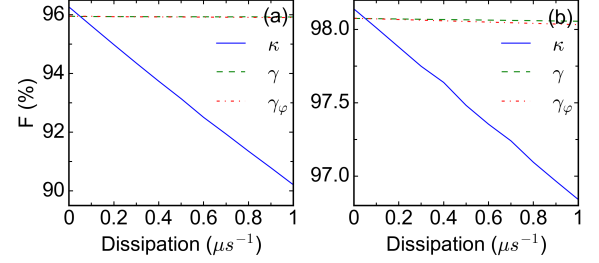


FIG. 11. The fidelity of the NS gate during the whole input and output process as a function of resonator dissipation κ (γ and γ_ϕ fixed at $0.05 \mu s^{-1}$), qubit damping γ (κ and γ_ϕ fixed at $0.05 \mu s^{-1}$) and dephasing γ_ϕ (γ and κ fixed at $0.05 \mu s^{-1}$). (a) Input state $\frac{1}{\sqrt{3}}(|0\rangle_w + |1\rangle_w + |2\rangle_w)$ consists of Lorentz wavepackets with bandwidth 0.02 GHz. (b) Input state $\frac{1}{\sqrt{3}}(|0\rangle_w + |1\rangle_w + |2\rangle_w)$ consists of Lorentz wavepackets with bandwidth 0.15 GHz.

one. We plot the input and output single-photon part waveform in Fig. 10 (a), whose overlap reaches 99.3%.

When the Lorentz wavepacket bandwidth reaches 0.15 GHz, the whole input and output process can be done in 70 ns, because a larger bandwidth indicates a stronger waveguide-resonator interaction, as shown in the right panel of Fig. 9. $g_{wr}/2\pi = 7.3 \exp(-0.24t)$ MHz, and $|\phi\rangle$ can be transferred into the resonator in $t_{in} = 20$ ns. After interaction with the qubit in $t_q = \sqrt{2}\pi/g_0 = 2.8$ ns, we increase $g_{wr}/2\pi$ linearly to 2.26 MHz. Finally, the photonic state is released to the waveguide with almost the same waveform as $|\phi\rangle$. The single-photon part input and output waveform is shown in Fig. 10 (b), whose overlap reaches 98.5%.

Finally, we consider the decoherence effects during the whole process. Now the interaction time is much longer than previous sections, so the effect of environment is more remarkable. We define fidelity $F = |\langle \psi_{ideal} | \rho_{out} | \psi_{ideal} \rangle|$ with $|\psi_{ideal}\rangle = \frac{1}{\sqrt{3}}|0\rangle_r(|0\rangle_w - |\tilde{1}\rangle_w - |\tilde{2}\rangle_w)$ and plot its relation with decoherence in Fig. 11. It is more sensitive to κ than to γ since the SQUID is populated for the longest duration, considering the transfers from and to the TL. Now one has to deal with a high dimensional ($\approx N^2/2$) density matrix in the master equation, so one may reduce N if the computer resource is

limited.

VI. CONCLUSION

We have presented a deterministic scheme for the two-photon nonlinear sign gate using variants of the two-photon QRM, which can be implemented in circuit QED. Initially, we consider the strong coupling regime. The nonlinearity is introduced through resonant interactions between microwave photons and a superconducting qubit, taking the form of a second-order nonlinear coupling. Subsequently, we construct a deterministic two-photon C-Z gate using the KLM scheme, which is robust against decoherence sources under current experimental conditions. We also achieve the C-Z gate in the p-USC regime and C-phase gate in the large detuning regime with specific parameters by analyzing the dynamics, which operates fast and remains robust despite imperfect experimental conditions. Finally, we show that the photonic state in the waveguide can be transferred into the resonator through a variable coupler, and re-

leased with almost the same waveform after interaction with the qubit, with a π -phase shift implemented. Our results offer a novel approach to realizing deterministic two-photon C-Z gates with the two-photon QRM and are expected to contribute to the advancement of quantum computing with microwave photons.

ACKNOWLEDGMENTS

The authors thank Jie-Qiao Liao, Zhi-hui Peng, Xun-wei Xu and Jin-Lei Tan for their helpful discussions. L. L. acknowledges the support from grants PID2022-136228NB-C21 and PID2022-136228NB-C22 funded by MCIN/AEI/10.13039/50110001103 and “ERDF A way of making Europe”, the Ministry for Digital Transformation and of Civil Service of the Spanish Government through the QUANTUM ENIA project call - Quantum Spain project, and by the European Union through the Recovery, Transformation and Resilience Plan - NextGenerationEU within the framework of the “Digital Spain 2026 Agenda”.

-
- [1] M. A. Nielsen and I. L. Chuang, *Quantum Computation and Quantum Information* (Cambridge University Press, Cambridge, UK, 2010).
 - [2] L. K. Grover, Quantum Mechanics Helps in Searching for a Needle in a Haystack, *Phys. Rev. Lett.* **79**, 325 (1997).
 - [3] T. D. Ladd, F. Jelezko, R. Laflamme, Y. Nakamura, C. Monroe and J. L. O’Brien, Quantum computers, *Nature* **464**, 7285 (2010).
 - [4] E. Knill, R. Laflamme and G. J. Milburn, A scheme for efficient quantum computation with linear optics, *Nature* **409**, 6816 (2001).
 - [5] J. L. O’Brien, A. Furusawa, and J. Vučković, Photonic quantum technologies, *Nature Photonics* **3**, 12 (2009).
 - [6] J. L. O’Brien, Optical quantum computing, *Science* **318**, 5856 (2007).
 - [7] S. Shi, B. Xu, K. Zhang, G.-S. Ye, D.-S. Xiang, Y. Liu, J. Wang, D. Su, and L. Li, High-fidelity photonic quantum logic gate based on near-optimal Rydberg single-photon source, *Nat. Commun.* **13**, 4454 (2022).
 - [8] D. Kielpinski, C. Monroe, and D. J. Wineland, Architecture for a large-scale ion-trap quantum computer, *Nature* **417**, 6890 (2002).
 - [9] N. A. Gershenfeld and I. L. Chuang, Bulk spin-resonance quantum computation, *Science* **275**, 5298 (1997).
 - [10] D. Press, T. D. Ladd, B. Zhang and Y. Yamamoto, Complete quantum control of a single quantum dot spin using ultrafast optical pulses, *Nature* **456**, 7219 (2008).
 - [11] L. M. Duan and H. J. Kimble, Scalable photonic quantum computation through cavity-assisted interactions, *Phys. Rev. Lett.* **92**, 127902 (2004).
 - [12] P. Krantz, M. Kjaergaard, F. Yan, T. P. Orlando, S. Gustavsson and W. D. Oliver, A quantum engineer’s guide to superconducting qubits, *Appl. Phys. Rev.* **6**, 021318 (2019).
 - [13] X. Gu, A. F. Kockum, A. Miranowicz, Y. X. Liu and F. Nori, Microwave photonics with superconducting quantum circuits, *Phys. Rep.* **718**, 1 (2017).
 - [14] F. Arute *et al.*, Quantum supremacy using a programmable superconducting processor, *Nature* **574**, 505 (2019).
 - [15] Y. Wu, W. S. Bao, S. Cao, F. Chen, M. C. Chen, X. Chen, *et al.*, and J. W. Pan, Strong Quantum Computational Advantage Using a Superconducting Quantum Processor, *Phys. Rev. Lett.* **127**, 180501 (2021).
 - [16] H. S. Zhong *et al.*, Quantum computational advantage using photons. *Science* **370**, 6523 (2020).
 - [17] J. Koch *et al.*, Charge-insensitive qubit design derived from the Cooper pair box, *Phys. Rev. A* **76**, 042319 (2007).
 - [18] F. Yoshihara *et al.*, Superconducting qubit–oscillator circuit beyond the ultrastrong-coupling regime, *Nat. Phys.* **13**, 44 (2017).
 - [19] A. Blais, A. L. Grimsmo, S. M. Girvin and A. Wallraff, Circuit quantum electrodynamics, *Rev. Mod. Phys.* **93**, 025005 (2021).
 - [20] H. Azuma, Quantum computation with Kerr-nonlinear photonic crystals, *J. Phys. D* **41**, 025102 (2007).
 - [21] L. S. Costanzo *et al.*, Measurement-induced strong Kerr nonlinearity for weak quantum states of light, *Phys. Rev. Lett.* **119**, 013601 (2017).
 - [22] L. Lamata, D. R. Leibbrandt, I. L. Chuang, J. I. Cirac, M. D. Lukin, V. Vuletić and S. F. Yelin, Ion Crystal Transducer for Strong Coupling between Single Ions and Single Photons, *Phys. Rev. Lett.* **107**, 030501 (2011).
 - [23] D. E. Chuang, V. Vuletić and M. D. Lukin, Quantum nonlinear optics — photon by photon, *Nat. Photonics* **8**, 685 (2014).
 - [24] B. Hacker, S. Welte, G. Rempe and R. Stephan, A photon–photon quantum gate based on a single atom in an

- optical resonator, *Nature* **536**, 7615 (2016).
- [25] P. Adhikari, M. Hafezi and J. M. Taylor, Nonlinear Optics Quantum Computing with Circuit QED, *Phys. Rev. Lett.* **110**, 060503 (2013).
- [26] Z. Chen, Y. Zhou and J. T. Shen, Deterministic Two-photon Controlled Phase Gate By Exploiting Nonlinear Pi-Phase Shift in Photonic Molecule Generations, *Advances in Photonics of Quantum Computing, Memory, and Communication XII*. Vol. 10933. SPIE (2019).
- [27] Z. Chen, Y. Zhou, J. T. Shen, P. C. Ku, and D. Steel, Two-photon controlled-phase gates enabled by photonic dimers, *Phys. Rev. A* **103**, 052610 (2021).
- [28] R. Li, J. Qian and W. Zhang, Proposal for practical Rydberg quantum gates using a native two-photon excitation, *Quantum Sci. Technol.* **8**, 035032 (2023).
- [29] M. Chen, J. S. Tang, M. Cai, Y. Lu, F. Nori, and K. Xia, High-dimensional two-photon quantum controlled phase-flip gate, *Phys. Rev. Res.* **6**, 033004 (2024).
- [30] D. Braak, Integrability of the Rabi Model, *Phys. Rev. Lett.* **107**, 100401 (2011).
- [31] Q.-H. Chen, C. Wang, S. He, T. Liu, and K.-L. Wang, Exact solvability of the quantum Rabi model using Bogoliubov operators, *Phys. Rev. A* **86**, 023822 (2012).
- [32] X.-Y. Lü, G.-L. Zhu, L.-L. Zheng, and Y. Wu, Entanglement and quantum superposition induced by a single photon, *Phys. Rev. A* **97**, 033807 (2018).
- [33] Z.-J. Ying, Symmetry-breaking patterns, tricriticalities, and quadruple points in the quantum Rabi model with bias and nonlinear interaction, *Phys. Rev. A* **103**, 063701 (2021).
- [34] Z.-M. Li and M. T. Batchelor, Generalized adiabatic approximation to the quantum Rabi model, *Phys. Rev. A* **104**, 033712 (2021).
- [35] J. Larson and T. Mavrogordatos, Jaynes-Cummings Model and Its Descendants: Modern Research Directions, IOP Series in Quantum Technology (IOP Publishing Ltd, Bristol, 2022).
- [36] J. Peng, J. C. Zheng, J. Yu, P. H. Tang, G. A. Barrios, J. X. Zhong, E. Solano, F. Albarrán-Arriagada, and L. Lamata, One-Photon Solutions to the Multiqubit Multimode Quantum Rabi Model for Fast W -State Generation, *Phys. Rev. Lett.* **127**, 043604 (2021).
- [37] J. Peng, J. N. Tang, P. H. Tang, Z. Z. Ren, J. L. Tian, N. Barraza, G. A. Barrios, L. Lamata, E. Solano, and F. Albarrán-Arriagada, Deterministic single-photon source in the ultrastrong-coupling regime, *Phys. Rev. A* **108**, L031701 (2023).
- [38] S. Felicetti, D. Z. Rossatto, E. Rico, E. Solano and P. Forn-Díaz, Two-photon quantum Rabi model with superconducting circuits, *Phys. Rev. A* **97**, 013851 (2018).
- [39] S. Felicetti, M. J. Hwang and A. Le Boité, Ultrastrong-coupling regime of nondipolar light-matter interactions, *Phys. Rev. A* **98**, 053859 (2018).
- [40] M. Ayyash, X. C. Xu, S. Ashhab, and M. Mariani, Driven multiphoton qubit-resonator interactions, *Phys. Rev. A* **110**, 053711 (2024).
- [41] I. Travenec, Solvability of the two-photon Rabi Hamiltonian, *Phys. Rev. A* **85**, 043805 (2012).
- [42] L. W. Duan, Y.-F. Xie, D. Braak and Q.-H. Chen, Two-photon Rabi model: analytic solutions and spectral collapse, *J. Phys. A: Math. Theor.* **49**, 464002 (2016).
- [43] S. Felicetti, J. S. Pedernales, I. L. Egusquiza, G. Romero, L. Lamata, D. Braak and E. Solano, Spectral collapse via two-phonon interactions in trapped ions, *Phys. Rev. A* **92**, 033817 (2015).
- [44] R. Puebla, M. J. Hwang, J. Casanova, and M. B. Plenio, Protected ultrastrong coupling regime of the two-photon quantum Rabi model with trapped ions, *Phys. Rev. A* **95**, 063844 (2017).
- [45] M. Hua, M. J. Tao, and F. G. Deng, Universal quantum gates on microwave photons assisted by circuit quantum electrodynamics, *Phys. Rev. A* **90**, 012328 (2014).
- [46] Y. Yin, Y. Chen, D. Sank *et. al.*, Catch and Release of Microwave Photon States, *Phys. Rev. Lett.* **110**, 107001 (2013).
- [47] J. E. Mooij, T. P. Orlando, L. Levitov, L. Tian, C. H. Van der Wal and S. Lloyd, Josephson Persistent-Current Qubit, *Science* **285**, 1036 (1999).
- [48] H. Zhang, S. Chakram, T. Roy *et. al.*, Universal Fast-Flux Control of a Coherent, Low-Frequency Qubit, *Phys. Rev. X* **11**, 011010 (2021).
- [49] P. Heidler *et al.*, Non-Markovian effects of two-level systems in a niobium coaxial resonator with a single-photon lifetime of 10 milliseconds, *Phys. Rev. Applied* **16**, 034024 (2021).
- [50] D. Bozyigit, C. Lang, L. Steffen *et. al.*, Antibunching of microwave-frequency photons observed in correlation measurements using linear detectors, *Nat. Phys.* **7**, 154 (2011).
- [51] D. M. Pozar, Microwave Engineering, 4th ed. (John Wiley & Sons, New York).
- [52] Z. Y. Ou, C. K. Hong, and L. Mandel, Relation between input and output states for a beam splitter, *Opt. Commun.* **63**, 2 (1987).
- [53] C. Lang *et al.*, Correlations, indistinguishability and entanglement in Hong-Ou-Mandel experiments at microwave frequencies, *Nat. Phys.* **9**, 345 (2013).
- [54] D. Z. Rossatto, C. J. Villas-Bôas, M. Sanz and E. Solano, Spectral classification of coupling regimes in the quantum Rabi model, *Phys. Rev. A* **96**, 013849 (2017).
- [55] S. P. Wang, G. Q. Zhang, Y. Wang, Z. Chen, T. Li, J. S. Tsai, S. Y. Zhu, and J. Q. You, Photon-Dressed Bloch-Siegert Shift in an Ultrastrongly Coupled Circuit Quantum Electrodynamical System, *Phys. Rev. Applied* **13**, 054063 (2020).
- [56] F. Beaudoin, J. M. Gambetta, and A. Blais, Dissipation and ultrastrong coupling in circuit QED, *Phys. Rev. A* **84**, 043832 (2011).
- [57] A. Ridolfo, M. Leib, S. Savasta, and M. J. Hartmann, Photon Blockade in the Ultrastrong Coupling Regime, *Phys. Rev. Lett.* **109**, 193602 (2012).
- [58] F. Mallet, F. R. Ong, A. Palacios-Laloy, F. Nguyen, P. Bertet, D. Vion and D. Esteve, Single-shot qubit readout in circuit quantum electrodynamics, *Nat. Phys.* **5**, 791 (2009).
- [59] A. Bengtsson, A. Opremcak, M. Khezri *et. al.*, Model-Based Optimization of Superconducting Qubit Readout, *Phys. Rev. Lett.* **132**, 100603 (2024).
- [60] J.-Q. Liao and C. K. Law, Correlated two-photon transport in a one-dimensional waveguide side-coupled to a nonlinear cavity, *Phys. Rev. A* **82**, 053836 (2010).
- [61] J.-Q. Liao and C. K. Law, Correlated two-photon scattering in cavity optomechanics, *Phys. Rev. A* **87**, 043809 (2013).
- [62] J. L. Tan, X. W. Xu, J. Lu, AND L. Zhou, Few-photon optical diode in a chiral waveguide, *Opt. Express* **30**, 28696 (2022).